Paper:
Jin, L., Li, L., Zhao, J. & Wang, D. (2019). Optical sensing interface based on nano-opto-electro-mechanical systems. *Sensors and Actuators A: Physical, 295*, 374-379.
http://dx.doi.org/10.1016/j.sna.2019.06.007

Accepted Manuscript

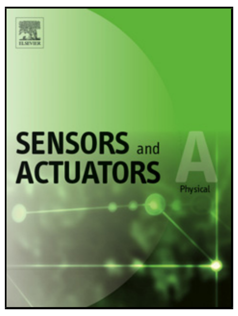

Title: Optical Sensing Interface Based on Nano-opto-electro-mechanical Systems

Author: Leisheng Jin Lijie Li Jiang Zhao Debo Wang

PII: S0924-4247(19)30448-0
DOI: https://doi.org/doi:10.1016/j.sna.2019.06.007
Reference: SNA 11427

To appear in: *Sensors and Actuators A*

Received date: 15 March 2019
Revised date: 6 June 2019
Accepted date: 6 June 2019

Please cite this article as: Leisheng Jin, Lijie Li, Jiang Zhao, Debo Wang, Optical Sensing Interface Based on Nano-opto-electro-mechanical Systems, *<![CDATA[Sensors & Actuators: A. Physical]]>* (2019), https://doi.org/10.1016/j.sna.2019.06.007

Optical Sensing Interface Based on Nano-opto-electro-mechanical Systems

Leisheng Jin[1*], Lijie Li[2], Jiang Zhao[1] and Debo Wang[1]

1. College of Electronic and Optical Engineering, Nanjing University of Posts and Telecommunications, Nanjing 210023, China;

2. Multidisciplinary Nanotechnology Centre, College of Engineering, Swansea University, Swansea SA1 8EN, United Kingdom.

Abstract

A novel optical sensing interface based on nano-opto-electro-mechanical systems (NOEMS) is proposed, in which the light can be coupled with quantum tunneled electrons via weak mechanical coupling. By taking optical pump power and mechanical coupling strength as varying parameters, respectively, bifurcation diagrams of three involved dynamical states of the NOEMS, i.e., optical, electrical and mechanical mode, are calculated, from which an effective coupling region for tunneled electrons and light is revealed. Self-oscillation, transient dynamics and the threshold of the NOEMS are further characterized, and it is found that the effective coupling region has a special transient time. The work sheds light in developing ultra-sensitive photon detectors using physical mechanisms rather than the conventional PN junction based.

Keywords: optical detector, quantum tunneling effect, nonlinear dynamics, resonator

1. Introduction

Nano-opto-electro-mechanical systems (NOEMS) are widely explored in developing highly efficient/low-noise transducers[1, 2], ultra-sensitive sensors[3, 4], quantum-limited measurement[5], optomechanical entanglement[6], multi-physics interfaces[7], optofluidics sensors[8] and etc.. To design NOEMS, mature techniques in the research field of optomechanics can be employed for realizing desired coupling between optical field and mechanics[9, 10, 11]. However, to achieve the coupling between optical and electrical fields in NOEMS, traditional ways of photoelectric conversion are still indispensable[12, 13, 14]. In certain circumstances, these traditional ways may bring drawbacks such as low sensitivity, circuit redundancy and read-out difficulties[15, 16]. Currently, much efforts are being made to solve these concerns[17]. For example, C. Bekker et al. have designed an integrated electrical interface in a cavity-based optomechanical system for providing direct electrostatic force[18], and in which the signal of the inertial drive and the reference injection signal can be locked. Recently, T. Bagci et al. use a high-quality silicon nitride (SiN) membrane to form a mechanically compliant capacitor in an optomechanical system, and by integrating the capacitor with resonant circuit the weak radio-frequency signals injecting on the membrane can be detected[19].

Here, a novel NOEMS serving as an optical sensing interface is proposed, in which the coupling between optical and electrical field is realized by using a pair of weakly coupled nanomechanical beams. In the pair, one acts as a part of an optical resonance cavity, and the other acts as movable part for forming the so-called nanomechanical transistor[20]. The proposed NOEMS, compared with traditional ones, is more compact and compatible with current MEMS/NEMS fabricating techniques. Particularly, the NOEMS is of the capability to capture the weak laser radiation pressure, and transfer the effect into electrical signal (tunneled electrons) directly, without any additional circuit. Theoretically, in characterizing the proposed NOEMS, subtle interplay between optical and electrical fields are for the first time revealed that there is an effective coupling region for tunneled electrons and lasers existing, and subsequently it is found that the transient time of this effective region is distinctive. The theoretical analysis shows that our proposed NOEMS can be developed as optical detectors and transducers.

2. Theoretical Model

As shown in Fig.1 (a), the proposed NOEMS consists of two nanomechanical beams. There are two ends of beams are mechanically coupled via an overhang, and the other two ends can vibrate freely. On the top of the left beam there is an metallic island G fabricated, and adjacent to G there are another two electrodes, source (S) and drain (D), are anchored. In working process, when a voltage is applied between S and D, a number of electrons can load from S to G and from G to D through quantum tunneling effect, coming into the so-called shuttle regime[20]. The beam on the right hand has a mirror fabricated on the top, which, together with another fiber Bragg

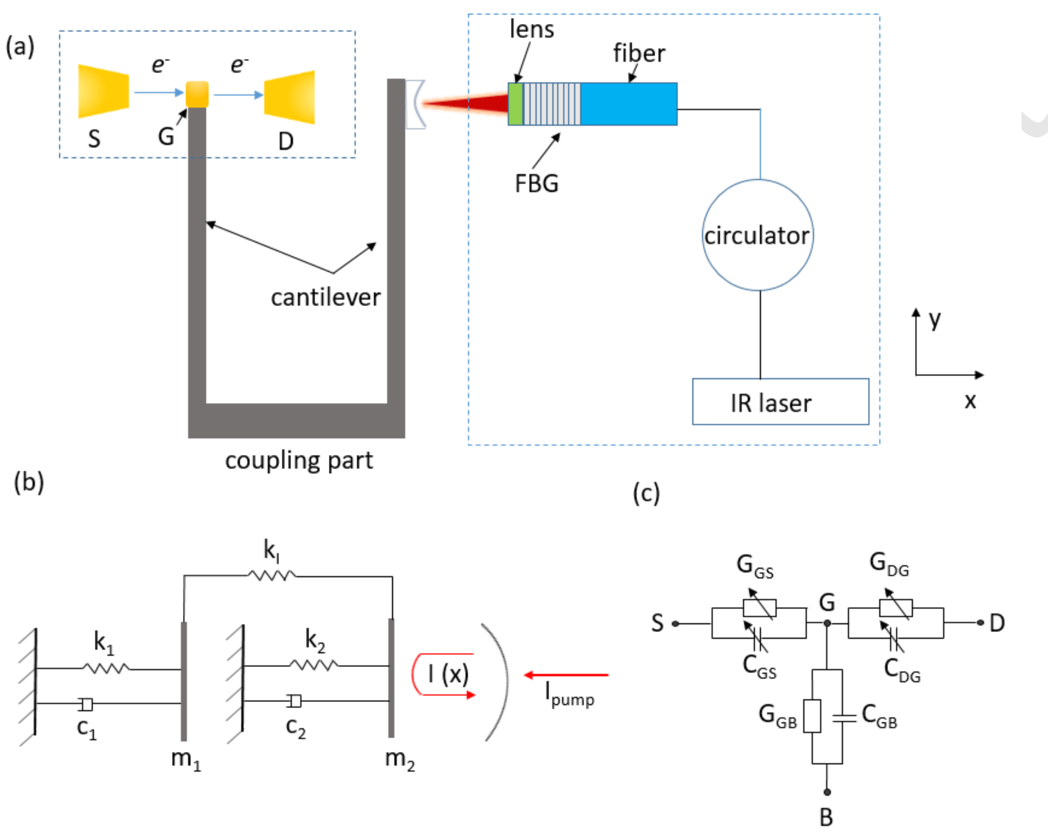

Figure 1: (a) Schematic diagram of the proposed NOEMS. (b) Lumped model of the proposed NOEMS. (c) Equivalent circuit of the electrical part in proposed NOEMS.

grating (FBG) working as a stationary mirror, creates an optical resonance cavity. A tunable infrared laser is then used for pumping the cavity. Under optical pumping, the beam on the right is subjected to a direct radiation pressure F_{rp}, and a thermal force F_{th} that originates from temperature change of the mirror. A lumped model illustrating how the two beam are coupled is given in Fig.1 (b), where $k_{1(2)}$ and $c_{1(2)}$ are spring constant and damping ratio, respectively, $m_{1(2)}$ represents the effective mass of the beam, and k_i denotes the mechanical coupling strength between the two beams. $I(x)$ is the intra-cavity optical power incident on the mirror, which depends on the displacement of right beam. Mathematically, the optical power I can be written as: $I(x_2) = (I_{max}(\frac{\Gamma}{2})^2)/(\frac{L^2}{2\pi^2}[1 - cos2\pi\frac{x_2-x_0}{L}] + (\frac{\Gamma}{2})^2)$, where L is the distance between two successive resonant positions of the nanomechanical mirror and

Γ represents the full width at half maximum parameter. x_0 is the position at which the energy stored in the optical cavity reaches a local maximum in steady state. x_2 is displacement of the right beam. I_{max} denotes the optical power after resonant enhancement, which is given by $I_{max} = C_{re}I_p$, where C_{re} is ratio of the resonant enhancement of the intra-cavity power and I_p is the power of the monochromatic light incident on the cavity. The equivalent circuit for describing the electromechanical part of the NOEMS is given in Fig.1 (c), where a capacitor in parallel with a tunnel conductance are adopted to model the tunnel junctions of $S-G$, $G-D$ and $B-G$, e.g., G_{GS} and C_{GS} are conductance and capacitance between terminal G and S. It should be noted that these conductances and capacitances excluding G_{GB} and C_{GB} all depend on the displacement of x_1. Specifically, $C_{GS,DG} = C^0_{GS,DG}(g/(g \pm 2x_1))$, $G_{GS,DG} = G^0_{GS,DG}e^{\mp x_1/\lambda}$, where $C^0_{GS,DG}$ and $G^0_{GS,DG}$ are initial capacitances and conductances, respectively, and g represents the gap between $S(D)$ and G. λ is the quantum tunneling length defined by $\lambda \approx (\frac{2\sqrt{2m_e\varphi}}{\hbar})^{-1}$. Here, m_e is the effective mass of a single electron, $\hbar$ is the Planck constant divided by 2π, φ is the work function of the electrode.

By treating the two nanomechanical beams as oscillators with a single degree of freedom, the NOEMS can be modeled as:

$$\ddot{x}_1 + \frac{\beta}{m_1}\dot{x}_1 + \omega_1^2 x_1 + \frac{k_i(x_1 - x_2)}{m_1} = \frac{V_D - V_S}{gm_1}Q_G \tag{1}$$

$$\ddot{x}_2 + \frac{\beta}{m_2}\dot{x}_2 + \omega_2^2 x_2 + \frac{k_i(x_2 - x_1)}{m_2} = \frac{F_{rp}}{m_2} + \frac{F_{th}}{m_2} \tag{2}$$

, where β is damping coefficient for both oscillators, $\omega_{1,2} = (B/L_{1,2})^2\sqrt{(EI_m)/(\rho A)}$, $(B = 1.875)$ is resonance frequency of the oscillator assuming same cross sectional area A ($w_1 = w_2$, $d_1 = d_2$) of the two cantilevers, and they are made of the same material with same Young's modulus E and density ρ. I_m is the moment of inertia, which is identical for the two beams.

In Eq. 2, the thermal force F_{th} is related to the variation of effective temperature T[22], i.e., $F_{th} = \theta(T - T_0)$, where θ is a coefficient of proportionality and T_0 is the temperature of the supporting substrate for right beam. The dynamical effective temperature T can be modeled by: $\dot{T} = -\kappa(T - T_0) + \eta I(x_2)$, where κ and η are effective thermal conductance and effective radiation absorption coefficient, respectively. The radiation pressure F_{rp} in Eq.2 directly depends on the optical power $I(x_2)$, i.e., $F_{rp} = \nu I(x_2)$, where $\nu = 2/c$ with c as the velocity of light.

In Eq.1, the charge on island G is changing dynamically as the left beam oscillating. Its dynamics can be derived from the Fig. 1 (c) that the charge variation at terminal G is the sum of electrical currents from terminals S, D and B, which can be expressed as:

$$\dot{Q}_G = V_D G^0_{DG} e^{-x_1/\lambda} + V_S G^0_{GS} e^{x_1/\lambda} + V_B G_{GB} - V_G(Q_G) G_\Sigma \tag{3}$$

, where

$$V_G(Q_G) = \frac{Q_G + V_D C_{DG} + V_S C_{GS} + V_B C_{GB}}{C_\Sigma} \tag{4}$$

and

$$C_\Sigma = C_{DG} + C_{GS} + C_{GB} \tag{5}$$

$$G_\Sigma = G^0_{DG} e^{-x_1/\lambda} + G^0_{GS} e^{x_1/\lambda} + G_{GB} \tag{6}$$

In addition, in Eqs.1 and 2, the resonance frequency ω_2 of the right beam is influenced by the effective temperature T. Given the the changes of temperature T is small, the relations between ω_2 and T can be expressed as: $\omega_2 = \omega_{20} - \delta(T - T_0)$, where the ω_{20} represents the fundamental resonance frequency of the right beam without optical pumping applied.

3. Numerical Analysis

Based on Eqs.1-6, numerical simulations are conducted. The parameters taken for numerical simulation are all experimentally acessed[21, 22]. Specifically, the length, width and thickness for the two beams in the NOMES are set to be identical: $L_1 = L_2 = 80$ nm, $W_1 = W_2 = 10$ nm and $T_1 = T_2 = 10$ nm. The material of the beams is chosen to be silicon with density $\rho = 2329$ kg/m^3. $\kappa = 7.3 \times 10^3$ 1/sec, $\theta = 4.7$ N/(kg$\cdot$ K), $T_0 = 77$ K, $x_0 = 10$ nm, Young's modulus $E = 140 \times 10^9$, $\eta = 7.5 \times 10^5$, $\lambda = 1 \times 10^{-10}$ m, $c = 3 \times 10^8$ m/sec, $L = 0.775 \times 10^{-6}$, $\gamma = 0.12 \times L$ and $\delta = 0.0001 \times \omega_1$. The effective mass $m_{(1,2)} = 3EI/(L^3_{(1,2)}\omega^2_{(1,2)})$, where $I_{(1,2)} = (W_{(1,2)}T^3_{(1,2)})/12$. The voltage applied to terminal B is $V_B = 6$ V. The initial gap between $S(D)$ and G is set to be 40 nm. The initial conductances of $G^0_{(GS,GD)}$ are taken to be $1/10^{10}$ S. $G^0_{GB} = 1/(6 \times 10^7)$ S. The initial capacitances C^0_{GS}, C^0_{DG} and C^0_{GB} are all taken to be 1×10^{-18} C. The damping ratios for two beams are taken to be 5×10^{-14} and 5×10^{-16}. Other parameters such as $V_{(S,D)}$, k_I, and I_p are taken as varying parameters. In addition, the displacement $x_{(1,2)}$ is calculated by using transformation relations $X_{(1,2)} = x_{(1,2)}/\lambda$.

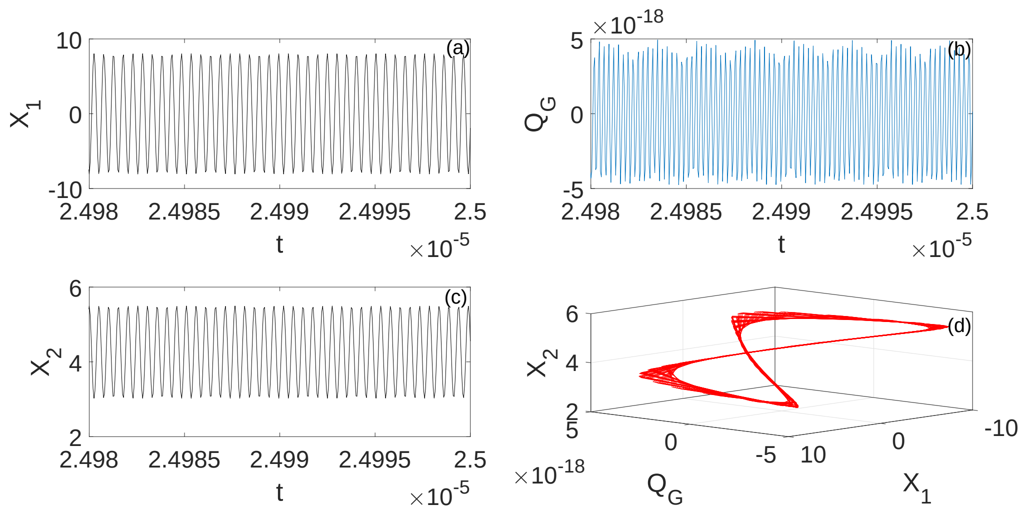

Figure 2: Self-excited oscillation of the proposed NOEMS when only optical pumping applied. (a) Displacement time series of the left oscillator. (b) The oscillation of charge on island G. (c) Displacement time series of the right oscillator. (D) Three-dimensional phase diagram of X_1, X_2 and Q_G.

3.1. Self-excited Oscillations

When there is only optical pumping applied, the NOEMS could work in self-excited oscillation under proper parameter settings. To confirm this, the Eqs.1 and 2 are first calculated based on given parameters, and by setting $V_S = -0.05$ V, $V_D = 0.05$ V, $k_i = 0.002$ and $I_p = 7.5$ mW. The numerical results is shown in Fig. 2, in which the time series of x_1, x_2 and Q_G are plotted. It is seen that the displacements of the two beams are oscillating stably. Here, the amplitude of the left oscillator is approximately 1 nm and the amplitude of the right oscillator is about 0.5 nm. The charge on the G is, however, oscillating periodically but with multi-amplitudes. This is due to the charge dynamics on G is of high sensitivity on the displacement of x_1, which, essentially, holds multiple but unnoticeable amplitude discrepancy. The number of the electrons shuttled between terminal S and D is approximately 35. In addition, a 3-D phase diagram plotting of the three involved dynamical states (X_1, X_2 and Q_G) is presented in Fig. 2 (d), in which a stable limit cycle is shown, again for proving the existence of the self-oscillation in the NOEMS.

3.2. Bifurcation diagram by taking optical power and coupling strength as variables

3.2.1. Optical Power

By setting $V_{(S,D)} = \mp 0.05$ V and fixing $k_i = 0.002$, the bifurcation diagram of three dynamical states (X_1, X_2 and Q_G), are investigated as the laser pump power I_p varying in [5 10] mw with the results shown as in Fig. 3 (a), (b) and (c). In order to better understand the bifurcation diagrams, it is of priority to conduct involved force analysis. The radiation force F_{rp} and thermal force F_{th}, which are closely related to the optical power I_p, act directly on the right beam. The electrostatic force: $F_e = (V_S - V_D)/2g \cdot Q_G$ acts on the left beam. The left and right beam are weakly coupled with a strength indexed by k_i. Thus, as the optical pumping power I_p increases, the right oscillator starts to make more impacts on the left one. First, let us see Fig. 3 (a), when I_p is relatively small, i.e., $I_p \in$[5 7] mW, the left oscillator is dominant by F_e that it is oscillating almost independently. The scattered points shown in Fig. 3 (a) in this range represent the peaks of the left oscillator working in transient state, and the peaks concentrated in the middle band come from the oscillations when the left oscillator reaches in stable states but with multiple amplitudes. As I_p increases to the range: $I_p \in$[7 8.4] mW (region 2), the impacts from the right oscillator is getting more powerful, and this can result in that the number of scatted peaks of the left are obviously reduced, which implies the effective coupling region for the optical pump and left beam coming to work. As the laser pump continues increasing to the range of $I_p \in$[8.4 10] mW, random large spikes of peaks appear. This is because the left beam at these points are terminated in transient state after a short lifetime. This phenomenon can be explained by that when the I_p increased to a certain level the influence from the right oscillator exerted on the left oscillator is so strong that the displacements of the left oscillator exceed the gap between terminals G and $S(D)$, which may fail the existing quantum tunneling effect. As the displacement of the left oscillator directly influence the charge dynamics of Q_G (see Eq. 3), it is therefore the bifurcation diagram of Q_G has the similar exhibition (Fig. 3 (b)) with I_p. The region 2 in Fig. 3 (b) implies that the light (laser) can be coupled with quantum tunneled electrons in the NOEMS. In Fig. 3 (c), the bifurcation diagram of X_2 with I_p varying in the range of [5 10] mW are also given, in which again three distinctive regions are revealed. In the first region, $I_p \in$[5 7] mW, there are more scatted peaks are distributed.

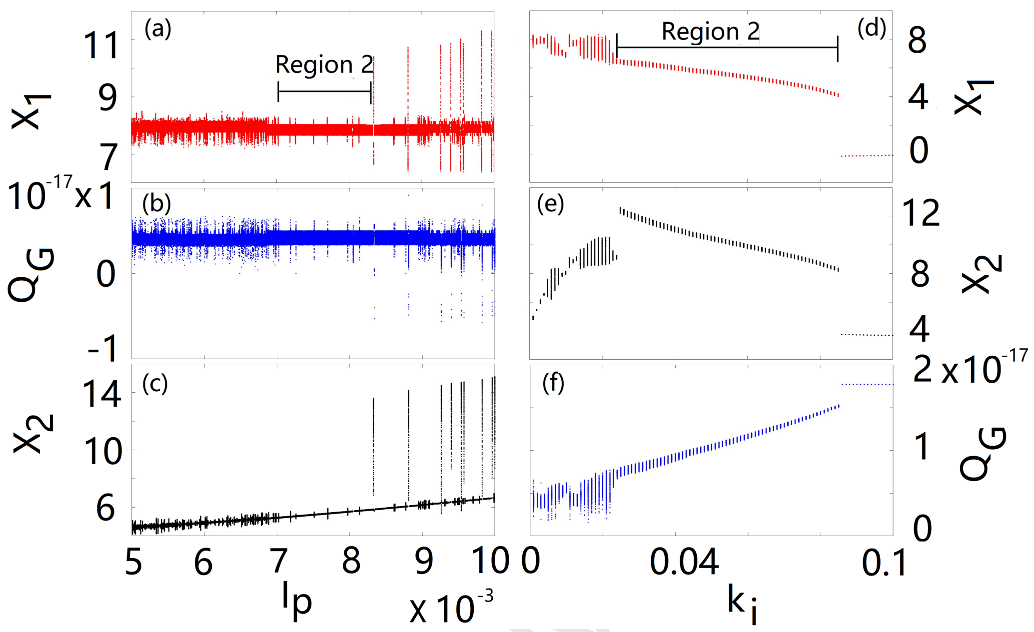

Figure 3: Bifurcation diagrams of the three involved states under varying optical pump driving I_P and mechanical coupling strength k_i. (a) The displacement X_1 vs I_p. (b) The charge on island G vs I_p. (c) The displacement X_2 vs I_p. Similarly, the bifurcation diagram with varying k_i: X_1 vs k_i in (d), X_2 vs k_i in (e) and Q_G vs k_i in (f).

In region 2, the peaks of the X_2 are getting more condensed. In the third region, similar phenomenon as shown in the Fig.3 (a)(b) is appeared. It is seen in Fig. 3 (c) that the average level of the peaks are gradually increased as the pumping, represented by I_p, is increasing. The correlations revealed in bifurcations diagrams shown in Fig.3 prove that there is an effective region existing for coupling external light with quantum tunneled electrons.

3.2.2. Coupling Strength

In the proposed NOEMS, the right and left beam are mechanically coupled. Here, we further conduct the analysis to investigate how the mechanical coupling strength k_i impact the three dynamical states. The results are shown in Fig. 3 (d), (e) and (f). During the calculation, the optical pumping power I_p is fixed to be 7.5 mW and $V_{(S,D)} = \mp 0.05$ V. The k_i is varied in the range of [0.001 0.1]. Overall, it is seen from the Fig. 3 (d, e, f) that each of bifurcation diagrams can be divided into three distinct regions. In the first region, when $k_i \in [0.001\ 0.023]$ the coupling strength between the two oscillators is relatively weak and the two oscillators are vibrating with more independence. There are more scatted peaks distributed, meaning the transient lifetime of the two oscillators is of randomness in this region. When k_i is increased to the second region (region 2), i.e., $k_i \in [0.023\ 0.082]$, the correlations of three involved dynamical states are getting more obvious, where the peaks values exhibit a strong correlation that the peaks values of X_1 and X_2 are decreasing while the the peaks values of Q_G are increasing. In the third region, when $k_i \in [0.082\ 0.1]$, the coupling strength between the two oscillators is strong enough that both oscillators' vibrations are terminated after a short transient process, and the charge Q_G stops tunneling between terminals S and D with around 110 electrons remaining on the electrode G.

3.3. Transient Dynamics

With the aim to better understand the system states dynamics, we further characterize the transient dynamics of the NOEMS. First, we study how the transient state of the left oscillator evolves into stable state when I_p setting in region 2, and a typical calculation of time series of X_1 when $I_p = 7.875$ mW is presented in Fig. 4 (a). In Fig. 4 (a), peaks findings of the oscillations are conducted twice, aiming to present a clear picture on how the dynamical process is changing. It is seen from the Fig. 4 (a) that the oscillation of the left beam goes though a transient period before reaching stable state, characterized by scatted peaks and single-valued peaks distributed, respectively. Second, we try to find at which point of I_p in the third region ($I_p \in [8.5\ 10]mW$) the peak spikes appears, and the results is given in Fig. 4 (b), where it is shown that when peak spikes occurring, indicated by the dashed lines, the number of the peaks is essentially dramatically decreased comparing with other I_p points, which confirms that at these special points of I_p the oscillation of the left beam is early terminated. Third, we pay our attention to the bifurcation diagram of Fig. 3 (d, e, f) trying to understand what the transient process of the left oscillator look like in terms of time series, and the result is given in Fig. 4 (c). In Fig. 4 (c), we conduct twice of peaks findings of the oscillations belonging to the left oscillator when $k_i = 0.007$. It is interesting to find that under weak mechanical coupling the dynamics of the left oscillator goes through rich bifurcations, including periodical to chaotic state, chaotical to periodical state, and single periodical to multi-periodical state. Forth, We deeply investigate how the optical pumping affects the transient state of the left oscillator. The result is given in Fig. 4 (d), in which it is revealed that the optical pumping power has an appar-

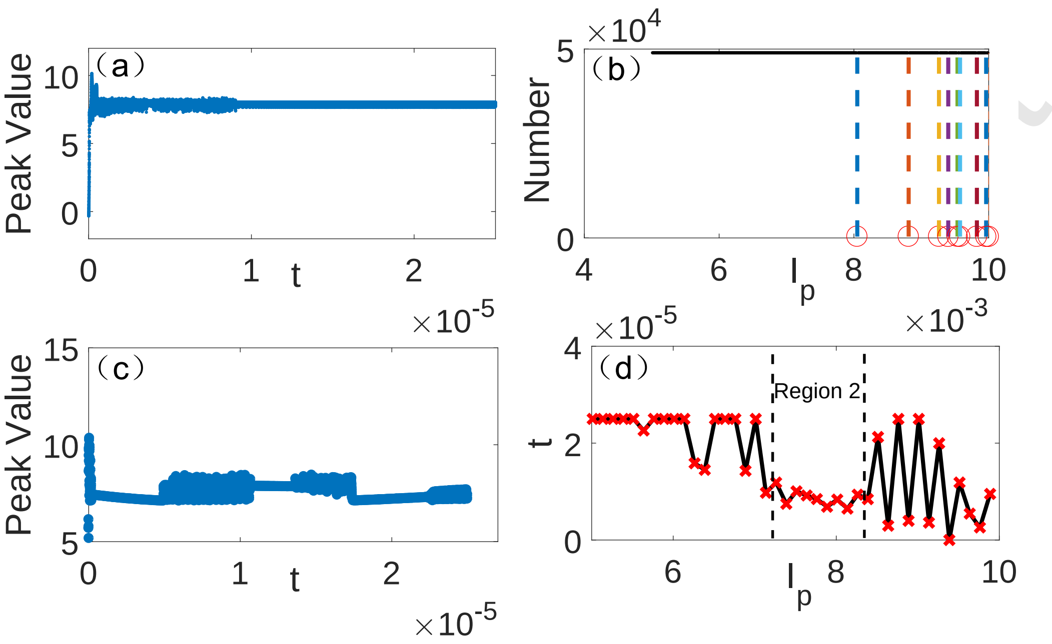

Figure 4: Transient dynamics of the proposed NOEMS. (a) Typical examples of how transient state of left oscillator evolves into stable periodical state when I_p in region 2. (b) The special points of I_p, indicated by dashed line, at which the spikes occurring in the bifurcation diagram Fig. 3. (c) Rich bifurcation phenomenon revealed when the two oscillators is weakly coupled with $k_i \in [0.001\ 0.023]$. (d) The lifetime of transient state under different optical pumping.

ent effect in modulating the lifetime of transient state of the left oscillator. Specifically, in the first region when $I_p \in [5\ \ 7]$ mW, the lifetime of transient state is relatively long and with less fluctuations, and in the region 2 when $I_p \in [7\ \ 8.5]$ mW the lifetime of transient state is reaching a lower level, while in the third region when $I_p \in [8.5\ \ 10]$ mW the lifetime of the transient state becomes more fluctuating. This phenomenon is in essential consistent with bifurcation study shown in Fig. 3, both confirming the proposed NOEMS is of capability for coupling the optical with quantum tunneled electrons.

3.4. Threshold Voltage and Optical Detectors

In addition to investigate the two key parameters (k_i and I_p) on how they make impact on the dynamics of the NOEMS, we also study the threshold of how much voltage needs to be applied to the source (S) and drain (D) electrodes for realizing the stable shuttling regime. Here, the optical pumping

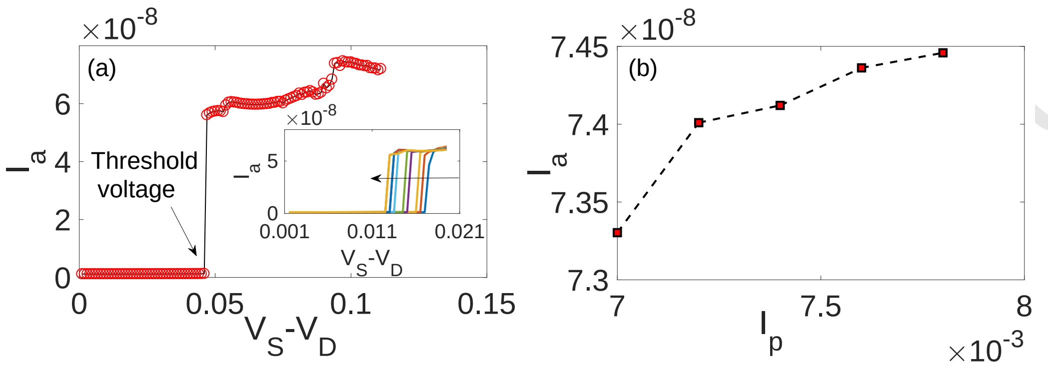

Figure 5: (a) Threshold at which shuttle regime starts and shuttle current appears. The subfigure shows the results of threshold under different mechanical coupling strength. (b) Proposed NOEMS works as an optical detector.

I_p is fixed to be 7.5 mW and $k_i = 0.002$, we try to find the threshold by calculating the average current I_a flowing between S and D. The current I_{SG} from S to G and $I_{D,G}$ from D to G can be obtained by using $I_{SG,DG} = (V_{S,D} - V_G)G_{SG,DG}$. The average current I_a is calculated in the range when voltage V_S (V_D) is increased from +0(-0) V to +0.08(-0.08) V, and the result is given in Fig. 5 (a), which clearly shows that it is not until the $V_S - V_D$ reaches about 0.046 V, there is an obvious current generating. After the threshold point, as the $V_S - V_D$ increasing, the output of current is slightly increased but with a fluctuating trend. The subfigure shown in Fig. 5(a) presents the results of the thresholds when mechanical coupling strength k_i varying in [0.0002 0.002]. It can be seen that the threshold value is decreasing while the k_i increases (arrow indicated). This is due to the energy localization phenomenon of weakly coupled beams. In Fig. 5(b), the result of using the proposed NOEMS for optical detection is given, which confirms that our proposed NOEMS can be used for optical detector and transducer. The NOEMS based optical sensing interface, therefore, can directly sense the light power, and transfer the optomechanical interaction into electrical signal.

4. Conclusion

In conclusion, a novel NOEMS that can couple optical and electrical field by using nanomechanical beams is proposed. The NOEMS is of capability to couple light with quantum tunneled electrons at nanosacle, which, therefore, may has potential in studying phonon-photon transfer physics in the quantum context. The distinct mechanism for photoelectric conversion in the proposed NOEMS could also be exploit in developing new type of single-photon detectors and ultra-sensitive sensors. Based on the theoretical analysis, rich nonlinear dynamics and subtle dynamical process are revealed, which provides theoretical basis for designing NOEMS-based optical sensing interfaces.

Acknowledgment

The author thank the support from National Natural Science Foundation of China (61604078; 51604157; 61704086); Natural Science Youth Foundation of Jiangsu Province(BK20160905); China Postdoctoral Science Foundation(2017M610341); Jiangsu Postdoctoral Science Foundation (1701044A).

References

[1] Leonardo Midolo, Albert Schliesser and Andrea Fiore, "Nano-opto-electro-mechanical systems," *Nature Nanotechnology* , vol. 13, pp. 11-18, 2018.

[2] Min Ren, Jianguo Huang, Hong Cai, Julius Minglin Tsai, Jinxiong Zhou,Zishun Liu, Zhigang Suo and Ai-Qun Liu, "Nano-optomechanical Actuator and Pull-Back Instability," *ACS Nano*, vol. 7, pp. 1676C1681, 2013.

[3] A. Tavernarakis, A. Stavrinadis, A. Nowak, I. Tsioutsios, A. Bachtold and P. Verlot, "Optomechanics with a hybrid carbon nanotube resonator," *Nature Communications*, vol. 9, pp. 662, 2018.

[4] O. Arcizet, P.-F. Cohadon, T. Briant, M. Pinard, A. Heidmann, J.-M. Mackowski, C. Michel, L. Pinard, O. Francais, and L. Rousseau, "High-Sensitivity Optical Monitoring of a Micromechanical Resonator with a Quantum-Limited Optomechanical Sensor," *Physical Review Letters*, vol. 97, pp. 133601, 2006.

[5] Shkarin, A. B. and Flowers-Jacobs, N. E. and Hoch, S. W. and Kashkanova, A. D. and Deutsch, C. and Reichel, J. and Harris, J. G. E., "Optically Mediated Hybridization between Two Mechanical Modes," *Physical Review Letters*, vol. 112, pp. 013602, 2014.

[6] Palomaki, TA, Teufel, JD, Simmonds, RW, Lehnert, K. W., "Entangling Mechanical Motion with Microwave Fields," *Science*, vol. 342, pp. 710-713, 2013.

[7] Zarko Zobenica, Rob W. van der Heijden, Maurangelo Petruzzella, Francesco Pagliano, Rick Leijssen, Tian Xia, Leonardo Midolo, Michele Cotrufo, YongJin Cho, Frank W.M. van Otten, Ewold Verhagen, Andrea Fiore, "Integrated nano-opto-electro-mechanical sensor for spectrometry and nanometrology," *Nature Communications*, vol. 8 (2216), pp. 1-8, 2017.

[8] Yuzhi Shi, Sha Xiong, Lip Ket Chin, Jingbo Zhang, Wee Ser, Jiuhui Wu, Tianning Chen, Zhenchuan Yang, Yilong Hao, Bo Liedberg, Peng Huat Yap, Din Ping Tsai, Cheng-Wei Qiu and Ai Qun Liu, "Nanometer-precision linear sorting with synchronized optofluidic dual barriers," *Science Advances*, vol. 4, eaao0773, 2018.

[9] Aspelmeyer, Markus; Kippenberg, Tobias J.; Marquard, Florian, "Cavity optomechanics," *Reviews of Modern Physics*, vol. 86, pp. 1391-1452, 2014.

[10] Yi Yang, Huiping Tian, Daquan Yang, Nannan Wu, Jian Zhou, Qi Liu, Yuefeng Ji, "Nanomechanical three dimensional force photonic crystal sensor using shoulder-coupled resonant cavity with an inserted pillar," *Sensors and Actuators A: Physical*, vol. 209, pp. 33-40, 2014.

[11] Tian-Xue Ma, Yue-Sheng Wang, Chuanzeng Zhang, Xiao-Xing Su, "theoretical research on a two-dimensional phoxonic crystal liquid sensor by utilizing surface optical and acoustic waves," *Sensors and Actuators A: Physical*, vol. 242, pp. 123-131, 2016.

[12] J. M. Taylor, A. S. Sorensen, C. M. Marcus, and E. S. Polzik, "Laser Cooling and Optical Detection of Excitations in a LC Electrical Circuit," *Physical Review Letters*, vol. 107, pp. 273601, 2011.

[13] Kejie Fang, Matthew H. Matheny, Xingsheng Luan and Oskar Painter, "Optical transduction and routing of microwave phonons in cavity-optomechanical circuits," *Nature Photonics*, vol. 10, pp. 489C496, 2016.

[14] Carlos Angulo Barrios, "A deflection optical sensor based on a Scotch tape waveguide with an integrated grating coupler," *Sensors and Actuators A: Physical*, vol. 269, pp. 500-504, 2018.

[15] J.-M. Pirkkalainen, S.U. Cho, F. Massel, J. Tuorila, T.T. Heikkila, P.J. Hakonen and M.A. Sillanpaa, "Cavity optomechanics mediated by a quantum two-level system," *Nature Communications*, vol. 6, pp. 6981, 2015.

[16] Jin, Leisheng; Ying, Lei; Yan, Xiaohong, "An Optical-Driven Quantum Shuttle: Modeling, Dynamics and Controllability ," *IEEE Jounal of Quantum Electronics*, vol. 54, pp. 9200107, 2018.

[17] Brian J. Roxworthy and Vladimir A. Aksyuk, "Nanomechanical motion transduction with a scalable localized gap plasmon architecture," *Nature Communications*, vol. 7, pp. 13746, 2016.

[18] Christiaan Bekker, Rachpon Kalra, Christopher Baker, and Warwick P. Bowen, "Injection locking of an electro-optomechanical device," *Optica*, vol. 4, pp. 1196-1204, 2017.

[19] T. Bagci, A. Simonsen, S. Schmid, L. G. Villanueva, E. Zeuthen, J. Appel, J. M. Taylor, A. Sorensen, K. Usami, A. Schliesser, "Optical detection of radio waves through a nanomechanical transducer," *Nature*, vol. 507, pp. 81C85, 2014.

[20] L. Y. Gorelik,A. Isacsson,M. V. Voinova,B. Kasemo,R. I. Shekhter,M. Jonson, "Shuttle Mechanism for Charge Transfer in Coulomb Blockade Nanostructures," *Physical Review Letters*, vol. 80, pp. 4526, 1997.

[21] Stav Zaitsev, Oded Gottlieb, Eyal Buks, "Nonlinear dynamics of a microelectromechanical mirror in an optical resonance cavity," *Nonlinear Dynamics*, vol. 69, pp. 1589-1610, 2012.

[22] Stav Zaitsev, Ashok K. Pandey, Oleg Shtempluck, and Eyal Buks, "Forced and self-excited oscillations of an optomechanical cavity," *Physical Review E*, vol. 84, pp. 046605, 2011.

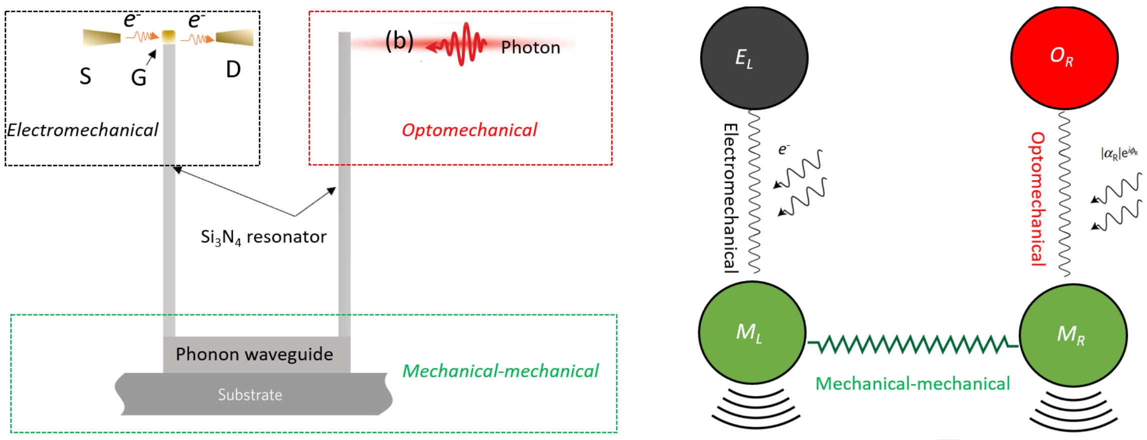

e⁻
e⁻
S
G
D
Electromechanical
(b)
Photon
Optomechanical
Si_3N_4 resonator
Phonon waveguide
Substrate
Mechanical-mechanical
E_L
O_R
Electromechanical
Optomechanical
M_L
M_R
Mechanical-mechanical

Highlight 1: The mechanism using ultra-sensitive quantum tunneling effect to capture rather weak optomechanical coupling due to light radiation pressure is one of highlights.

Highlight 2: Detailed nonlinear dynamics analysis reveals a distinctive region with special transient time in which light can be coupled with quantum tunneled electrons.

Highlight 3: The NOEMS based optical sensing interface could be developed into quantum regime for studding photon-phonon-electron interaction process.

Leisheng Jin received his Ph.D. degree in Nanotechnology from Swansea University, Wales, UK, in 2015. He is currently working as a full time associate professor in Nanjing University of Posts and Telecommunications, Nanjing, China. His research interests include: nonlinear dynamics in MEMS/NEMS, electron transportation in nanoscale devices, and dynamics/applications in optomechanics.